Available online at www.sciencedirect.com
SCIENCE DIRECT®
Composites: Part B 36 (2005) 271–277
composites Part B: engineering
www.elsevier.com/locate/compositesb

Characterization of nano and meso scale deformation structures with intense X-ray synchrotron sources

G.E. Ice, R.I. Barabash*, F.J. Walker

Metals and Ceramics Division, Oak Ridge National Laboratory, Oak Ridge, TN 37831-6118, USA

Received 1 June 2004; revised 28 September 2004
Available online 2 December 2004

Abstract

Advanced polychromatic microdiffraction is sensitive to the organization of dislocations and other defects that rotate the lattice planes. Using ultra-brilliant third-generation synchrotron sources and non-dispersive X-ray focusing optics, it is now possible to analyze individual dislocation cells and walls at a submicron scale that cannot be probed by traditional methods. The method is applied to an Ir weld sample to illustrate how microdiffraction can be used to determine the locally active dislocation system.
© 2005 Elsevier Ltd. All rights reserved.

Keywords: B. Plastic deformation; Defects; D. Non-destructive testing; E. Joints/joining; Analytical modeling

1. Introduction

Polychromatic X-ray microdiffraction offers a fundamentally new approach to the study of mesoscale dynamics in polycrystalline materials [1–3]. As a polychromatic X-ray beam penetrates a sample, it produces a Laue pattern from each subgrain that it intercepts (Fig. 1a). The method has major advantages over traditional monochromatic diffraction for micron and submicron scale spatial resolution because no sample rotations are required and the depth at which the scattering originates can be resolved through a newly described differential aperture microscopy technique [2].

In addition to providing precise information on the phase, grain orientation and morphology of polycrystalline materials, polychromatic microdiffraction is sensitive to elastic and plastic strain. As illustrated in previous papers, the deviatoric or full elastic strain tensor can be recovered from single and polycrystalline materials with X-ray micro-Laue methods [2–4]. It has also been shown previously that quantitative information on the number and kind of unpaired random dislocations can be recovered from streaking in the Laue images [5]. A general kinematic treatment of polychromatic X-ray scattering by crystals with dislocations was presented in Ref. [5]. Here we summarize the key features of the earlier paper and extend the approach to cases where the dislocations are organized into dislocation walls. With this formalism, the diffraction from plastically deformed materials with random unpaired dislocations, dislocation walls or combinations of unpaired dislocations and dislocation walls can all be modeled. Welded sample grains show interesting deformation that depends on the thermal history of a grain and on the local boundary conditions. Previous studies of deformation have been attempted in these materials based on Electron Backscatter Diffraction (EBSD) methods [6], however, until recently, non-destructive three-dimensional analysis of plastic deformation with micron resolution was not possible for bulk materials. Here we illustrate how the 12 most likely dislocation systems produce distinctive streaking in a polychromatic microdiffraction image and how the measured streaking can be used to quantitatively determine the local deformation tensor of a subgrain volume in an Ir weld.

2. Multiscale dislocation structure

It is known that plastic deformation involves several structural levels [7]. At the first level, there are individual

* Corresponding author. Tel.: +1 865 241 7230; fax: +1 865 574 7659.
E-mail address: barabashr@ornl.gov (R.I. Barabash).

1359-8368/$ - see front matter © 2005 Elsevier Ltd. All rights reserved.
doi:10.1016/j.compositesb.2004.10.001

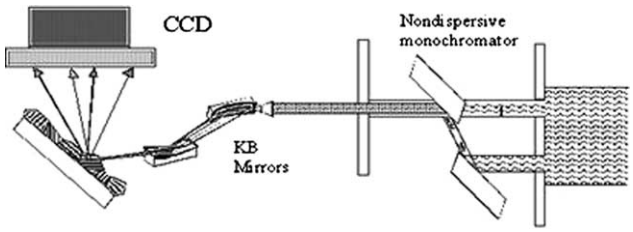

Fig. 1. Experimental set-up for white beam Laue diffraction.

dislocations in the volume with typical size l_1: $\sqrt{n^{-1}} > l_1 > b$ (where n is dislocations density, b is Burgers vector). As a result of the strong interaction between dislocations, a random dislocation distribution becomes unstable and forms a correlated dislocation arrangement with screening radius l_2 due to grouping of dislocations into dislocation walls. Some fraction of the dislocations may remain randomly distributed and the rest form various correlated dislocation and disclination arrangements. The size of the second structural level is defined by equation: $D_{\text{cell}} > l_2 > \sqrt{n^{-1}}$ and typically on the nano-scale. Neighbouring cells are usually separated by 'so called' incidental dislocation boundaries (IDBs). The typical distance between adjacent IDBs defines the cell size ($D_{\text{cell}} \sim 50$–500 nm). The next structural level involves fragments. Fragments with the size D_{fr} contain cells with approximately the same crystallographic orientation $D_{\text{fr}} > l_3 > D_{\text{cell}}$. Geometrically necessary boundaries (GNBs) separate two fragments. For crystals with unpaired tilt dislocation walls (GNBs or IDBs), X-ray diffraction spots are broadened in proportion to the number of excess dislocations inside the wall and to the total number of unpaired walls.

The next structural level l_4 is related to the typical grain size D_{gr}: $D_{\text{gr}} > l_4 > D_{\text{fr}}$. At the macroscopic level l_5 with typical size $l_5 > 10D_{\text{gr}}$ individual defects are ignored and solids can be treated as continuous media with some elastic–plastic properties.

Classic X-ray methods usually average over a large number of grains and give ensemble-average information related to the 3rd or 4th structure level. With white-beam microdiffraction it is possible to quantitatively analyze a sample at all structure levels described above. In particular, it is now possible to analyze details of structure corresponding to nano- and mesoscopic levels. No other probe can study such a wide range of length scale.

We wish to model the influence of deformation structure on X-ray microdiffraction images. We adopt the concept of cell-block structure first introduced by Mughrabi et al. [8] and further developed in a number of papers (see for example Ref. [9]). We restrict ourselves to models where the unpaired edge dislocations have one of three organizations: (1) random geometrically necessary (unpaired) dislocations (GNDs); (2) unpaired geometrically necessary boundaries (GNBs) formed by thin dislocations walls; (3) GNB's separating regions with incidental dislocation boundaries (IDB) and individual geometrically necessary dislocations (GNDs). A sketch of these structures is presented at Fig. 2.

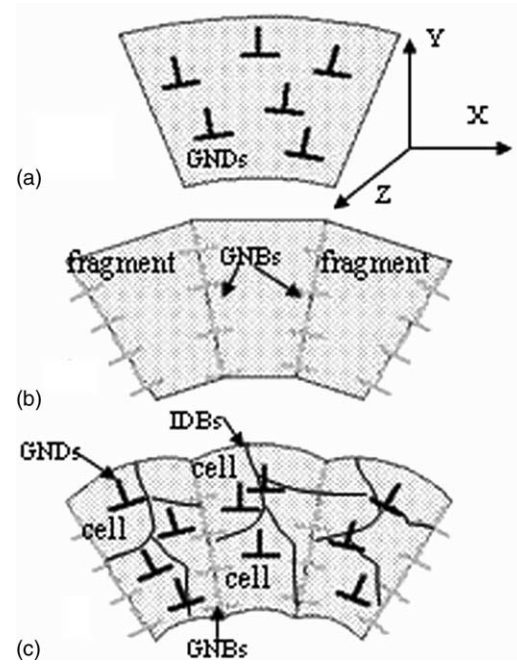

Fig. 2. Models of crystals with different arrangement of unpaired dislocations: a—randomly distributed individual unpaired dislocations; b—randomly distributed tilt dislocation walls; c—randomly distributed tilt dislocation walls with randomly distributed individual unpaired dislocations in inner regions.

Consider the set of edge dislocations illustrated in Fig. 2. Dislocations from this set have Burgers vectors, $\mathbf{b}_i$, parallel to the X-axis and dislocations lines, $\boldsymbol{\tau}$ parallel to the Z-axis. For an equal number of random '$+\mathbf{b}$' and '$-\mathbf{b}$' dislocations, the average deformation tensor is negligible. Broadening of the diffuse scattering is induced by random local fluctuations in the unit cell orientations and d spacing that tend to cancel out over long length scales.

To describe the distribution of dislocations, we introduce the number c_t. It can take two values:

$$c_t = \begin{cases} 1, (+) \\ 0, (-) \end{cases}.$$

If there is a dislocation in the position t, the corresponding number $c_t = 1$, and in positions without dislocations $c_t = 0$. Each edge dislocation creates a displacement field with displacement $\mathbf{u}_{it}$ of the i-th scattering cell in the plane XOY perpendicular to its line. The projections of the displacement vector in this plane for the simple case of elastically isotropic crystals, are described by the following equations [10,11].

$$u_x = \frac{b}{2\pi}\left[\tan^{-1}\frac{y}{x} + \frac{xy}{2(1-\mu)(x^2+y^2)}\right] \tag{1a}$$

$$u_y = -\frac{b}{2\pi}\left[\frac{1-2\mu}{2(1-\mu)}\ln(x^2+y^2) + \frac{(x^2-y^2)}{4(1-\mu)(x^2+y^2)}\right] \tag{1b}$$

Here μ is Poisson's ratio. The total displacement of the i-th cell $\mathbf{u}_i$ is due to superposition of all dislocations and is defined by the equation [12]

$$\mathbf{u}_i = \sum_t c_t \mathbf{u}_{it} \tag{2}$$

The tensor of dislocation density $\rho_{\tau n}$ has indices τ that specify the crystallographic direction of the dislocation line, and the index n that specify the Burgers vector direction. For a general set of dislocations with dislocation density ρ_0, line directions parallel to the plane normal lmn, and Burgess vector $l'm'n'$ we write the tensor of dislocation density as,

$$\rho_{\tau n} = \begin{pmatrix} \rho_{oll'} & \rho_{olm'} & \rho_{oln'} \\ \rho_{oml'} & \rho_{omm'} & \rho_{omn'} \\ \rho_{onl'} & \rho_{onm'} & \rho_{onn'} \end{pmatrix} \tag{3}$$

For unpaired edge dislocations as shown in Fig. 2a, $\tau=(001)$, $n=(100)$ mean deformation tensor has only two non-zero components $\omega_{xy}=-\omega_{yx}=n^+bx$. We note that this distortion field is antisymmetric and represents a pure rotation about the Z-axis that increases with displacement in x. Other systems of edge, screw or mixed dislocations can be similarly treated, but for the following discussion we restrict ourselves to edge dislocations.

In real crystals individual GNDs tend to group into walls to reduce the stored energy [8–12]. Consider a structure with geometrically necessary randomly distributed tilt dislocation boundaries (GNBs) (Fig. 2b). Each wall provides a rotation between two neighboring mosaic blocks around the line of the wall. The unit vector $\boldsymbol{\omega}$ parallel to the rotation axis of each wall coincides with the unit vector $\boldsymbol{\tau}$ along the dislocation lines in the case of a tilt boundary. We consider pure tilt boundaries formed by equidistant edge GNDs (so called 'thin walls'). These boundaries do not produce long-range elastic strain but generate subgrain rotations. The remaining stresses in the GNB region are periodic with a wavelength $b^*=b\csc\Theta/2$. These stresses are only appreciable at distances shorter than within b^* from the GNB [10]. If h is the distance between these dislocations in the wall, one can consider the boundary as a single defect producing the local rotation field Θ. The misorientation angle Θ due to the boundary is defined by the equation $b/h=2\sin\Theta/2$ where $b/h\approx\Theta$ for small angle GNB's. To characterize this model quantitatively we define the average distance D between GNBs and write the number of GNBs per unit length as $1/D$. The total density of GNDs grouped in the GNBs is denoted by $n^+=1/Dh$. We define an axis X perpendicular to the plane of the wall, and an axis Z parallel to the direction of dislocation lines in the wall. For this coordinate system, (Fig. 2) two non-zero components of the mean deformation tensor are equal: $\omega_{xy}=-\omega_{yx}=\Theta x/D$. This mean deformation tensor again results in pure rotations about the Z axes. The rotations increase with displacement in x. The number of GNBs per unit length and the length of the crystal in the X direction determines the total rotation of the lattice.

Generally, real crystals contain a hierarchy of dislocation structures. Some of the GNDs are distributed randomly, and the rest may form different non-random arrangements: IDBs and GNBs. It has been found that dislocation boundaries evolve within a regular pattern of grain subdivision on two scales [8–12]. The smaller scale is related to cell boundaries called incidental dislocation boundaries (IDBs). These boundaries exist within larger scale boundaries called GNBs (Fig. 2c). IDBs may be paired or unpaired. GNBs are larger scale typically unpaired or have larger misorientations.

3. Laue diffraction by nano- and meso-scale dislocations structure

3.1. Formation of Laue Image

In traditional white-beam Laue diffraction, a continuum spectrum is diffracted by a single crystal (or single grain) [13]. The crystal scatters the beam into a characteristic Laue pattern that depends on the crystal space lattice, its orientation and the incident-beam energy distribution (Fig. 1). Each characteristic reflection hkl is scattered specularly from the crystal planes hkl, which allows the planar orientations with respect to the incident beam to be determined directly. The initial spectral distribution can be described by $I_0(k)$ where $(k=|\mathbf{k}_0|)$. In reciprocal space the exact positions of regular reflections (hkl) are related to the orientation, space lattice and of the real-space unit cell size. The momentum transfer corresponding to a Bragg/Laue reflection we define as, $\mathbf{G}_{hkl}=k_{hkl}-k_0$, where $(|\mathbf{k}_0|=|\mathbf{k}_{hkl}|=k)$. Here k_0 is the incident wave vector and k_{hkl} is the scattered wave vector that satisfies the Bragg/Laue conditions. The diffuse scattering intensity depends on the deviation $\mathbf{q}=\mathbf{Q}-\mathbf{G}_{\mathrm{hkl}}=\mathbf{k}-\mathbf{k}_{\mathrm{hkl}}$ between the diffraction vector $\mathbf{Q}=\mathbf{k}-\mathbf{k}_0$, and the momentum transfer G_{hkl} for a Laue reflection. For each wavelength, the center of the Ewald sphere (C) and the origin in reciprocal space (O) are separated by the distance $1/\lambda$. This distance is different for each reflection hkl and corresponds to different Ewald spheres; this complicates the analysis for polychromatic beams. We write the Laue equation in a manner that takes into account the spectrum of λ in the beam. Pixel positions on the CCD are converted into q space (sample basis) using the geometrical calibration parameters of the CCD relatively to the incoming beam (distance, center channel, tilts of detector). Indexing provides the unit cell orientation with respect to a model basis. A rotation matrix is then used to go from the sample to the unit cell basis. In non-distorted crystals each Laue reflection with incident beam $\mathbf{k}_0$

and the diffracted beam $\mathbf{k}_{hkl}$ determine the direction of Bragg plane normal $\mathbf{G}_{hkl}$ [4,14,15]. The Bragg plane normal and 2ϑ angle for each reflection are fixed and compared to possible pairs of indices for crystal structure. To simplify the computation for indexing, we project the reciprocal lattice directions onto the q_x, q_y plane. This projection, as opposed to a more standard stereographic projection, is used for the analysis of experimental results in Figs. 4, 5.

3.2. Streaking of Laue spots due to unpaired dislocations and dislocation walls

Dislocations change the diffraction conditions and enlarge the region of high intensity around each Bragg position. The region of high intensity around each reciprocal lattice vector G_{hkl} in Laue geometry I_L is a function of a misorientation vector $\mathbf{m} = \hat{\mathbf{k}} - \hat{\mathbf{k}}_{hkl}$. The misorientation vector $\mathbf{m}$ gives the difference between the unit vector parallel to Bragg reflection (h,k,l) and an arbitrary direction in its vicinity. Within this approximation, the resulting intensity distribution by the deformed crystal in the white microbeam method can be written as:

$$I_L(\mathbf{m}) = A\int I_0(k)I(\mathbf{q})\mathrm{d}k;$$
$$\mathbf{q} = |\mathbf{k}_{hkl}|\mathbf{m}_{\perp} + (|\mathbf{k}_{hkl}|\mathbf{m}_{\mathrm{rad}} + \Delta k\mathbf{G}/|\mathbf{k}_{hkl}|) \tag{4}$$

Here $|k_{hkl}|$ is the radius of the Ewald sphere that passes through G_{hkl}, and A is a constant. Eqs. (1a) and (1b) is valid when $\frac{\Delta k}{|k_0|} \ll 1$. In the first approximation, the orientation vector m is perpendicular to k_{hkl}. The intensity distribution $I(q)$ of X-ray (or neutron) scattering due to defects can be computed from the expression

$$I(\mathbf{Q}) = |\sum_i f_i \exp(i\mathbf{Q}\cdot(\mathbf{R}_i^0 + \mathbf{u}_i))|^2. \tag{5}$$

Here f_i is the scattering factor from an individual atom i, with relaxed co-ordinates $R_i = \mathbf{R}_i^0 + \mathbf{u}_i$ due to the presence of defects. Here u_i is the displacement from the equilibrium positions $\mathbf{R}_i^0$ corresponding to the crystal before deformation defined by Eq. (2). The intensity distribution of a crystal with dislocations may be written as follows [5,12,16].

$$I(\mathbf{q}) = f^2 \sum_{i,j} \mathrm{e}^{i\mathbf{q}\cdot\Delta}\mathrm{e}^{-T} \quad T = nS\sum_t 1 - \mathrm{e}^{(i\mathbf{Q}\cdot(\mathbf{u}_{it}-\mathbf{u}_{jt}))} \tag{6}$$

Here f is the average scattering factor; $\Delta = \mathbf{R}_i^0 - \mathbf{R}_j^0$ is the distance vector between the lattice cells i, j in the undistorted virtual crystal; S is the area of one dislocation in a transverse plane; n is the total dislocation density, and nS is a dimensionless quantity that indicates the fraction of lattice sites covered with dislocations. The correlation function T differs for different dislocation arrangements. In the most general case it contains both real and imaginary parts. If all dislocations are paired, the imaginary part is equal to zero and the correlation function T is real. If there are unpaired (GND) dislocations the function T contains both real and imaginary parts.

The correlation function T, can be expanded with respect to small displacements and has both real and imaginary parts. The first term T_1 is imaginary and is linear with respect to x and n^+. The real part of the correlation function T_2 is the same as for paired dislocations:

$$T_1 = -iC_1 \sum_\lambda n_\lambda^+(\mathbf{R}_i\cdot\mathbf{b}_\lambda)([\mathbf{Q} * \mathbf{R}_{ij}]\boldsymbol{\tau}_\lambda);$$
$$T_2 = C_2(Qb)^2 \ln L \sum_\lambda n_\lambda \varphi_\lambda \tag{7}$$

Here C_1, C_2 are the contrast factors, λ is the number of the dislocation slip system, L is the size of the subgrain (or the cut off radius), ϕ_λ is the orientation factor for each dislocation system. From the structure of this equation it follows that dislocations parallel to the diffraction vector do not contribute to the function T_1 and do not influence the intensity of scattering (contrast factor C_1 for these dislocations is zero). T_1 describes the influence of mean distortions due to randomly distributed individual GNDs.

For an equal number of random '$+\mathbf{b}$' and '$-\mathbf{b}$' dislocations the broadening of the diffuse scattering is induced by random local fluctuations in the unit cell orientations and d spacing that tend to cancel out over long length scales. Due to the character of the displacement field around edge GNDs, displacements occur only in planes perpendicular to the direction of dislocation lines $\boldsymbol{\tau}$. As a result, coherence is not changed along the direction $\boldsymbol{\tau}$, and the diffuse intensity in this direction is the same as for crystals without dislocations. Perpendicular to $\boldsymbol{\tau}$, the diffuse distribution is roughly symmetric with a characteristic full width at half maximum (FWHM) dependent on the total dislocation density n: FWHM $\propto \sqrt{n}$. For GNDs (Fig. 2), the diffuse scattering distribution relates the distortion tensor, ω_{ij}, due to GNDs, n^+, to the dislocation density and system (direction $\boldsymbol{\tau}$, and Burgers vector $\mathbf{b}$). For $\boldsymbol{\tau}||Z$ and $\mathbf{b}||$ to X there are only two non-zero components of the mean deformation tensor: $\omega_{xy} = -\omega_{yx} = n^+bx$. We note that this distortion field is antisymmetric and represents a pure rotation about the Z axis that increases with displacement in x. Arbitrary systems of edge or screw dislocation can be similarly treated, but for the following discussion we restrict ourselves to edge dislocations.

3.3. Splitting of Laue spots

If the distance between GNBs is sufficiently large, the reflection becomes discontinuous. To understand this dependence, we assume that along the penetration depth L the X-ray beam intersects several fragments with average size D_{fr}. Each fragment contributes to the diffraction. The number of such contributions is equal L/D. Each boundary produces average misorientation Θ. The average distance between the Laue maximums, formed by two adjacent

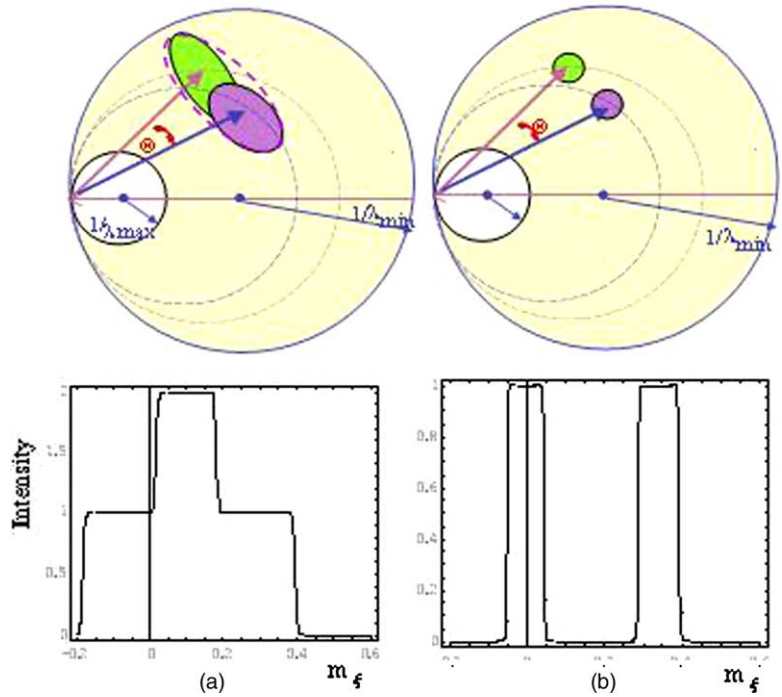

Fig. 3. Model (top) and simulated intensity profiles (bottom) for split Laue reflections diffracted from two fragments for two extreme values of the criterion (8): (a) continuous distribution ($K<1$), (b) Spot splits into separate spikes ($K>1$).

fragments is $\Delta=(Q/k_0)\Theta$. If this distance exceeds the average $\mathrm{FWHM_{fr}}$ of the Laue image for each fragment along the ξ axis, the Laue spots split. If almost all dislocation walls are unpaired, the following criterion can be used:

$$K=\left(\frac{\Theta Q}{k_0\mathrm{FWHM_{fr}}}\right) \tag{8}$$

If $K<1$, the intensity distribution of white beam reflection is continuous, if $K>1$ the white beam reflection is split into separate spots. The intensity profile along the streak consists of several spikes. With higher resolution the experimental intensity distribution reveals more spikes (Fig. 3). The results of simulated scattering by general dislocation structures (when some fraction of dislocations is grouped into the walls and some of them are randomly distributed in the inner regions) are illustrated in the next section.

Unpaired boundary and individual dislocations can have either similar or distinctive effect on the Laue pattern. Both of them result in streaking of Laue reflections. The same orientation of GNDs and GNBs correspond to the same direction of streaking. However, GNDs cause continuous and GNBs discontinuous intensity distributions along the streak. Due to local strains, individual dislocations influence the length of the streak more than the same number of dislocations in a boundary. Moreover the FWHM, in the narrow direction of the streak is most strongly influenced by individual dislocations and can be used to separate boundary dislocations from the ones inside the fragment. For better separation of unpaired boundary and individual dislocations, the white X-ray microbeam intensity should be differentiated with respect to $|\mathbf{k}_0|$. Scanning the incident X-ray energy with an incident beam monochromator can do this. The differentiated results provide a true 3D volume in reciprocal space as opposed to a 2D projection of line integrals as with a simple Laue pattern. The results of simulated scattering by general dislocation structures (when some part of dislocations is grouped into the walls and some of them are randomly distributed in the inner regions) are illustrated in the next section.

3.4. Multi-scale dislocation structure near an Ir weld

The microbeam-Laue technique was applied to a complicated dislocation structure arising from plastic deformation in an *Ir* weld. As shown below (Figs. 4 and 5) welding of polycrystalline *Ir* can be accompanied by

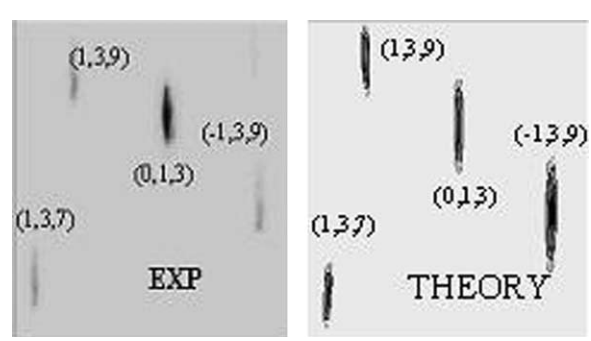

Fig. 4. Experimental (a) and simulated (b) Laue patterns from *Ir* weld in the heat affected zone.

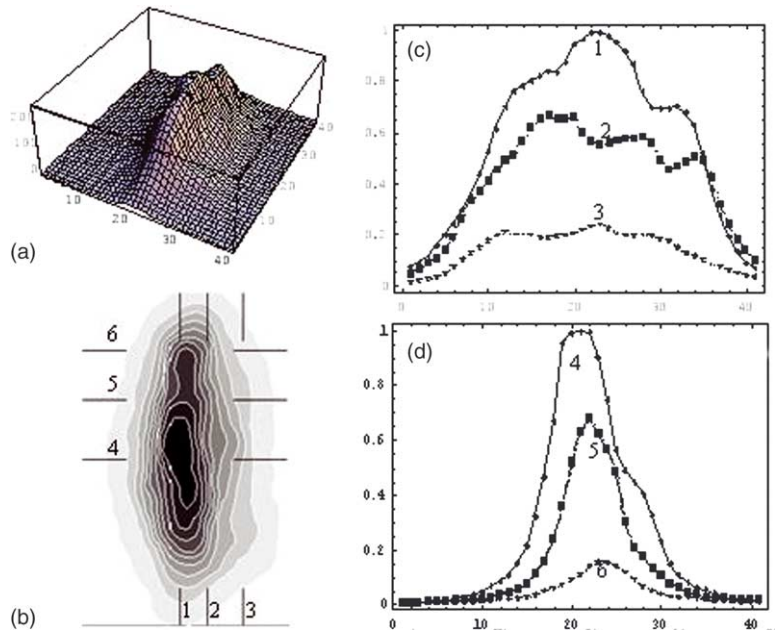

Fig. 5. (a) Three dimension representation of (013) Laue spot; (b) contour map; (c) three profiles parallel to streak direction ξ; (d) three profiles perpendicular to ξ illustrating bunching of the intensity into several spikes.

local plastic deformation as well as by residual stress [17]. Microbeam-Laue diffraction reveals pronounced streaking of Laue images in the heat affected zone. The plastic response of the material in the heat affected zone can be described by the formation of geometrically necessary dislocations (GNDs) that appear in the material to relax the stress field induced during welding and subsequent cooling. In FCC crystals, typical edge dislocation lines 'run' parallel to the direction of $\langle 112 \rangle$ with Burgers vector parallel to the direction $\langle 110 \rangle$ and with corresponding glide planes $\{111\}$ [10].

Laue images were made at different grains in the weld and in the heat affected zone. In the center of the weld, Laue spots are sharp indicating that there is no residual plastic or elastic strain. In the heat-affected zone large grains are observed with significant deformation. Experimental and simulated Laue patterns are shown at Fig. 4. The orientation of the grain surface normal presented at Fig. 4a was almost parallel to [013]. To understand the shape of experimental Laue images and to check the sensitivity of the Laue image to different possible dislocation orientations, we have chosen four central Laue spots for one of the grains in the heat-affected zone (Fig. 4). We simulated their Laue images corresponding to 12 different slip systems of the primary GNDs. The 12 most likely edge dislocation systems for this grain in the sample contribute distinct patterns to the beam spread. The qualitative and quantitative difference between the different systems allows for identification of the active dislocation system (Fig. 4b). It has Burgers vector $b = [01\bar{1}]$ dislocation line $\tau = [211]$ and slip plane $n = (\bar{1}11)$. The density of GNDs can be estimated by fitting the experimental Laue pattern by the simulated ones. A transition from one dislocation network to another is observed at various positions in the weld. The intensity profiles of virtually all Laue spots are discontinuous indicating the presence of GNBs. The 3D portrait, contourmap and several intensity profiles along X and Y directions of the streak are shown in Fig. 5 for a reflection (013). According to the Eq. (8) those profiles corresponds to a case when the criterion $K \sim 1$. At least some of the GNDs are grouped into dislocation walls forming geometrically necessary boundaries (GNBs). The presence of at least two pronounced boundaries separating three fragments in the irradiated volume is observed. Misorientation angles between the central and neighboring fragments are ~ 0.25 and 0.35°, for the left and the right fragment, respectively.

4. Summary

X-ray microdiffraction with broad-bandpass X-ray beams provides a powerful new tool for the study of plastic deformation in materials at nano- and mesoscopic levels. Plastic deformation with a primary set of unpaired (GND) dislocations results in elongated streaks in the Laue image that can be used to determine the dislocation density. Different slip systems cause a distinctly different streaking of Laue pattern. The intensity profile in different directions of the streak allows for separation between unpaired random dislocations, and unpaired dislocation cell walls and GNBs. The orientation and density of the primary dislocation systems are determined for a grain near a welded Ir joint. Misorientation created by each sub-boundary as well as average size of each fragment was determined at local scale.

Modeling of local plastic deformation is now needed to understand the mechanisms driving the observed dislocation structures.

Acknowledgements

Research sponsored by the Division of Materials Sciences and Engineering, Department of Energy, under Contract DE-AC05-00OR22725 with UT-Battelle, LLC. Measurements were performed at MHATT-CAT at APS also supported by DOE Office of Basic Energy Sciences.

References

[1] Ice GE, Larson BC. Adv Eng Mater 2002;2(10):643–6.
[2] Larson BC, Yang W, Ice GE, Budai JD, Tischler JZ. Nature 2002;415: 887–90.
[3] Margulies L, Winther G, Poulsen HF. Science 2001;291:2392–4.
[4] Chung JS, Ice G. J Appl Phys 1999;86(9):5249–55.
[5] Barabash R, Ice GE, Larson BC, Pharr GM, Chung K-S, Yang W. APL 2001;79:4.
[6] Field DP, Weiland H. In: Electron backscatter diffraction in materials science. New York: Kluwer Academic; 2002 pp. 199–212.
[7] Romanov AE, Vladimirov VI. In: Nabarro F, editor. Dislocations in solids, vol. 9. Amsterdam: North Holland; 1992. p. 191.
[8] Wilkens M, Ungar T, Mughrabi H. Phys Stat Sol (a) 1987;104: 157–70.
[9] Hughes DA, Hansen N. Acta Mater 2000;48:2985–3004.
[10] Nabarro FRN. Theory of crystal dislocations. New York: Dover Publications Inc; 1987.
[11] Humphreys FJ, Hatherly M. Recrystallization and related annealing phenomena. London: Pergamon; 1996.
[12] Krivoglaz MA. Theory of X-ray and thermal neutron scattering by real crystals. New York: Plenum Press; 1969.
[13] Shenoy GK, Viccaro PJ, Mills DM. Characteristics of the 7 GeV advanced photon source: a guide for users. Argonne, IL: Argonne National Laboratory; 1988. No.ANL-88-9.
[14] Tamura N, Celestre RS, MacDowell AA, Padmpre HA, Spolenak R, Valek BC, Chang NM, Manceau A, Patel JR. Rev Sci Instrum 2002; 73:1369–72.
[15] Lauridsen EM, Juul Jensen D, Poulsen HF, Lienert U. Scripta Mater 2000;43:561–6.
[16] Thomson R, Levine LE. Acta Cryst 1997;A53:590–602.
[17] Noyan IC, Cohen JB. Residual stress. New York: Springer; 1987.